



Effects of surface roughness on the propulsive performance of pitching foils

Rodrigo Vilumbrales-Garcia^{1,†}, Melike Kurt¹, Gabriel D. Weymouth^{1,2} and Bharathram Ganapathisubramani¹

¹Faculty of Engineering and Physical Sciences, University of Southampton, Southampton SO17 1BJ, UK

²Faculty of Mechanical, Maritime and Materials Engineering (3mE), TU Delft, Delft, 2628 CD, The Netherlands

(Received 10 January 2023; revised 23 October 2023; accepted 24 October 2023)

The hydrodynamic influence of surface texture on static surfaces ranges from large drag penalties (roughness) to potential performance benefits (*shark-like skin*). Although it is of wide-ranging research interest, the impact of roughness on flapping systems has received limited attention. In this work, we explore the effect of roughness on the unsteady performance of a harmonically pitching foil through experiments using foils with different surface roughness, at a fixed Strouhal number and within the Reynolds number (Re) range of 17 000–33 000. The foils' surface roughness is altered by changing the distribution of spherical-cap-shaped elements over the propulsor area. We find that the addition of surface roughness does not improve the performance compared with a smooth surface over the Re range considered. The analysis of the flow fields shows near-identical wakes regardless of the foil's surface roughness. The performance reduction mainly occurs due to an increase in profile drag. However, we find that the drag penalty due to roughness is reduced from 76% for a static foil to 16% for a flapping foil at the same mean angle of attack, with the strongest decrease measured at the highest Re . Our findings highlight that the effect of roughness on dynamic systems is very different than that on static systems; thereby, it cannot be estimated by only using information obtained from static cases. This also indicates that the performance of unsteady, flapping systems is more robust to the changes in surface roughness.

Key words: flow–structure interactions, swimming/flying, drag reduction

1. Introduction

Surface roughness is ever-present in engineering applications, involving complex fluid–structure interactions. Its implications on the flow and the consequent drag

† Email address for correspondence: rvglu19@soton.ac.uk

generation have been widely studied in the related literature. From the influence of roughness in pipe flow (Achenbach 1971), to its effects on the trajectory of a golf ball (Chowdhury *et al.* 2016), roughness plays a vital role in any application involving fluid–structure interaction considerations. For example, surface roughness can be detrimental to the performance of wind turbines. Sagol, Reggio & Ilinca (2013) found that the accumulation of contamination agents in the blades leads to a reduction in power extraction, whereas Ehrmann *et al.* (2017) reported a performance decrease linked to an increase in roughness density and height. On the other hand, the use of roughness elements can lead to a drag reduction and certain performance gains for unsteady propulsion systems. Previous studies inspired from swimmers and flyers show that, from shark skin or dolphin skin (Dean & Bhushan 2010) to feathers on a wing of a gliding bird (Van Bokhorst *et al.* 2015), roughness in varying shapes and texture modifies the fluid flow over propulsor surfaces, leading to a reduction in drag or a decrease in flow separation. In engineering applications, Gad-el Hak & Bushnell (1991) analysed the effects of roughness turbulators and found an increase in the ratio between the lift and the drag coefficient when compared with a smooth foil for chord-based Reynolds number lower than 100 000. In addition, the use of surface riblets can lead to a decrease in skin friction when aligned in the flow direction (Bechert *et al.* 1997), achieving a drag reduction of up to 8 % (Walsh 1982). An important roughness parameter to consider is the roughness Reynolds number H^+ , defined as $H^+ = Hu_\tau/\nu$ where H is the height of the rough element, ν is the kinematic viscosity and u_τ is the friction velocity. For H^+ values less than 70, the flow is usually characterised as transitionally rough. When $H^+ > 70$, the rough elements extend into the logarithmic region, the smooth-wall viscous sublayer is assumed to have been completely destroyed and the surface is considered to be fully rough (Bakken *et al.* 2005).

Recent studies have analysed the effects of superhydrophobic coating on the surface of pitching foils. Mallah *et al.* (2021) reported an increase in the lift and thrust production for a pitching foil at low Strouhal values when compared with a smooth foil, which could lead to improved manoeuvrability and propulsive efficiency.

When configured properly, surface roughness can be beneficial. It can reduce drag production and potentially improve the overall performance. Surface roughness can also have detrimental effects. Tailoring the surface roughness to have an improved performance requires a better understanding of the effect of shape, size and area distribution of roughness elements on both the force production and the flow.

The drag-reduction potential of surface roughness on aquatic swimmers have been explored mainly for static surfaces. For example, sharks can reduce their skin friction when their riblets are aligned with the flow (Dean & Bhushan 2010). Bixler & Bhushan (2013) pointed out that the riblets lift and pin the vortices generated in the viscous sublayer, leading to a decrease in drag. Bechert, Bruse & Hage (2000) observed a drag reduction for interlocking 3D riblets. Afroz *et al.* (2016) concluded that ‘shark-like’ textures can act like a passive flow separation control mechanism. Du *et al.* (2022) found smaller separated regions and adverse pressure gradients for the flow over a foil covered with tilted biomimetic shark scales. The effect of the shape and size of the rough elements were analysed by Domel *et al.* (2018a), highlighting the importance of the denticle shape, as they found a drag reduction only for the smaller of the three considered. Although surface roughness has shown promising potential for static bodies, its role in unsteady systems is still not clear. Shark-skin surfaces have been shown to increase the self-propelled swimming speed and reduce the drag of a flapping foil (Oeffner & Lauder 2012; Domel *et al.* 2018a), but only when small denticles are used, whereas the larger elements can lead to an increase in drag. Wen, Weaver & Lauder (2014) reported a reduction in energy

consumption due to a formation of stronger leading-edge vortices. Guo *et al.* (2021) found that, for steady foils, the roughness elements resulted in a considerably thicker boundary layer when compared with the smooth foil, whereas for dynamic foils, the changes due to roughness in the wake characteristics were considerably smaller. Mostly, previous work conclude that shark-inspired surfaces can improve the performance of an unsteady body, but the potential benefit is strongly dependent on the shape and size of shark denticles, which often appear in highly complex geometries. Therefore, it is still to be seen if such performance improvement can be achieved with simple, commercially available roughness elements, located on the surface of an unsteady foil in harmonic motions.

In this study, we analyse experimentally the effects of surface roughness on the propulsive performance of a pitching foil by using simple roughness elements. In § 2, we define the methodology and experimental set-up used to actuate three different foils with varying roughness characteristics. We investigate the effects of chord-based Reynolds number in the range of $17\,000 \leq Re \leq 33\,000$ and report the propulsive performance of a pitching hydrofoil in terms of thrust production (C_X) and efficiency (η). In § 3, we detail the force and flow measurement results obtained for flapping foils, and draw a comparison between dynamic and static foil cases.

2. Experimental set-up and methodology

Force and flow measurements are conducted in a recirculating water flume at the University of Southampton, with a test section of 8.1 m length, 1.2 m width and 0.9 m depth. A surface plate is installed at the foil tip and the foil is placed right above the bottom wall to prevent tip vortex formation and enforce nominally two-dimensional flow over the foil as shown in [figure 1\(a\)](#).

Three foils with a rectangular planform and a NACA0012 cross-section were 3-D-printed using polylactic acid (PLA) filaments with an infill density of 70 %, a chord-length of $c = 0.16$ m and an aspect ratio of $AR = 2.5$. Spherical-cap-shaped roughness elements with a width (diameter) of $W = 0.05c$ and height of $H = 0.01c$ (Domel *et al.* 2018b) were placed on pressure and suction sides of the foils. As shown in [figure 1\(c\)](#), in addition to the smooth foil, two different roughness levels are considered by varying the area occupied by the spherical-cap elements to 36 % and 70 % of the foil planform area. The rough elements were distributed in uniform streamwise rows on both sides of the foil to ensure symmetry, with the amount of rough elements designed to achieve the coverage areas defined before.

Each foil was actuated with a stepper motor (Applied Motions STM23S) in sinusoidal pitching motions, about a point $0.08c$ distance from the leading edge. The prescribed motion is defined by $\theta(t) = \theta_0 \sin(2\pi f_0 t)$, where θ_0 is the pitching amplitude and f_0 is the flapping frequency. The pitching amplitude θ_0 , Strouhal number $St = 2c \sin(\theta_0) f_0 / U$ and reduced frequency $k = 2\pi f_0 c / U$ were fixed all throughout the experiments at $\theta_0 = 7.5^\circ$, $St \approx 0.22$ and $k \approx 5.2$, in line with previous studies (Mackowski & Williamson 2015; Kurt & Moored 2018; Senturk & Smits 2019; Fernandez-Feria & Sanmiguel-Rojas 2020). A Reynolds number sweep ($Re = Uc/\nu$ where ν is the kinematic viscosity) was conducted within the range of $17\,000 \leq Re \leq 33\,000$ by varying the flow velocity, U . It has been reported in previous studies (Senturk & Smits 2019) that Re can have a major impact on the propulsive performance of a pitching foil, although as Re is increased over $Re = 16\,000$ the thrust production appears to reach a constant value. A summary of the parameters used in this study is given in [table 1](#).

The forces and moments acting on the foils were measured with a six-axis force sensor (ATI Gamma IP65). The motion was tracked using a rotary, incremental encoder (US

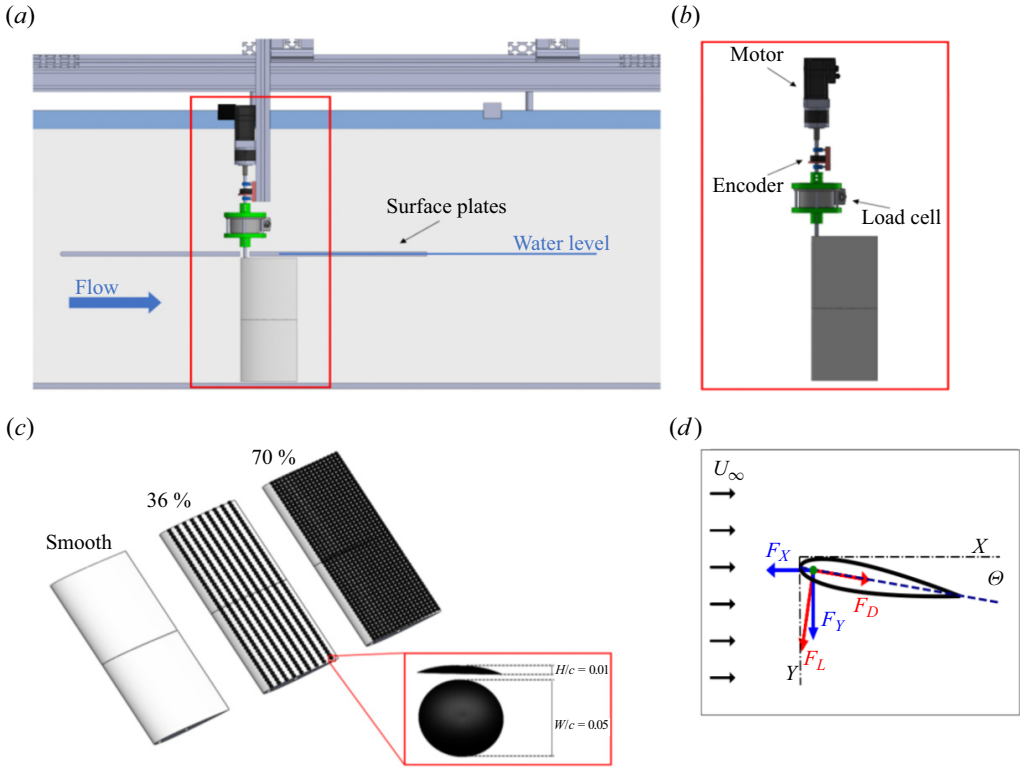


Figure 1. Schematics of the experimental set-up in the water flume (a), the actuation arm (b), foils with three different roughness area coverage ratio (c) and the forces acting on the foil (d).

| Re | 17 000 | 22 000 | 28 000 | 33 000 |
|---------------------------|--------|--------|--------|--------|
| U (m s^{-1}) | 0.12 | 0.15 | 0.19 | 0.23 |
| f_0 (Hz) | 0.62 | 0.80 | 1.00 | 1.20 |
| θ_0 (deg.) | 7.5 | 7.5 | 7.5 | 7.5 |

Table 1. Experimental parameters used in the current study.

Digital E5) attached to the motor shaft (figure 1b). Each trial was conducted for a total of 100 flapping cycles (where $t/T = 1$ cycle) and repeated five times. The measured forces were filtered using a Butterworth filter with a low-pass frequency of seven times the flapping frequency. The power was calculated as a multiplication of the pitching moment and the angular velocity, which was derived from the measured angular displacement. The instantaneous and time-averaged performance metrics are the average values from 500 flapping cycles, measured over five trials ($N = 5$). The confidence intervals are calculated following a t -distribution with 5 samples, as $\bar{x} \pm 4.60\sigma/\sqrt{N}$, where \bar{x} is the sample mean, σ is the sample standard deviation and N corresponds to the number of repetitions (five). To distinguish instantaneous forces from time-averaged results, the latter is denoted by $\overline{(\cdot)}$. The reported streamwise force (thrust) (C_X) and power (C_P) coefficients and efficiency (η)

are defined as

$$C_X = \frac{F_X}{\frac{1}{2}\rho U^2 s c}, \quad C_P = \frac{P}{\frac{1}{2}\rho U^3 s c}, \quad \eta = \frac{C_X}{C_P}, \quad (2.1a-c)$$

where ρ is the density of water, s is the hydrofoil span and U represents the free-stream flow velocity.

The force measurements were synchronised with planar particle image velocimetry (PIV) measurements (cameras, LaVision MX 4MP; lasers, Litron Nano PIV). The field of view captures the entire foil and up to one chord-length in the foil's wake. The software Davis 10 was used to cross-correlate the acquired particle image pairs (with 24×24 pixels with 50% overlap). The flapping cycle was divided into 22 phases and 25 cycles were acquired per phase. The velocity fields corresponding to each phase were then averaged over 25 cycles.

3. Results

3.1. Flow-field and force production analysis of foils with different roughness area coverage ratios

Figure 2 compares the out-of-plane vorticity and the instantaneous performance coefficients, C_X and C_P , for all the roughness cases considered at $Re = 28\,000$. The first column (*a,d*), the second column (*b,e*) and the third column (*c,f*) present the evolution of the vorticity field around three pitching foils with 0%, 36% and 70% surface roughness at $t/T = 0.15$ and $t/T = 0.50$, respectively. Surprisingly, change in the roughness does not lead to any significant alteration in the vorticity fields. Regardless of the roughness coverage, all foils produce a reverse von Kármán–Street where two counter-rotating vortices per flapping cycle are shed from the trailing edge into the wake, as widely observed in the related literature for smooth foils (Anderson *et al.* 1998; Schnipper, Andersen & Bohr 2009; Muscutt, Weymouth & Ganapathisubramani 2017; Kurt & Moored 2018). Figure 2(*g,h*) presents the evolution of cycle-averaged thrust and power coefficients over one flapping cycle. Similar to the flow fields, the performance coefficients show only minor differences between the smooth foil and the foils with roughness. Although we have only revealed the analysis associated with a single Re , these results hold across the Re range considered here. In the supplementary material available at <https://doi.org/10.1017/jfm.2023.1009>, we present the evolution of the flow field over one flapping cycle at $Re = 17\,000$ and $Re = 28\,000$ as videos for comparison. Overall, these results from force and flow field measurements show that incorporating surface roughness does not have a strong influence on the development of the wake. Other parameters, such as Strouhal number or kinematics (Schnipper *et al.* 2009), are known to significantly affect the evolution of the vortex structures, which can minimise the adverse effects on performance induced by the roughness elements.

Figure 3 introduces the spectral analysis conducted for the raw, pre-filtered C_X forces. The power spectra of the thrust force at $Re = 28\,000$ is shown in (*a*). The crosses indicate the location of the peak frequency for each foil. In (*b*), we introduce the dominant frequency ratio in the form of f/f_0 , where f_0 is the prescribed pitching frequency across the Re range considered. This analysis shows that the dominant frequency in thrust production corresponds to twice the pitching frequency f_0 for all the Re values and contains similar energy density for all the foils. This result, combined with the similarities observed in both the wake and the instantaneous forces, indicates that the performance of the foils is

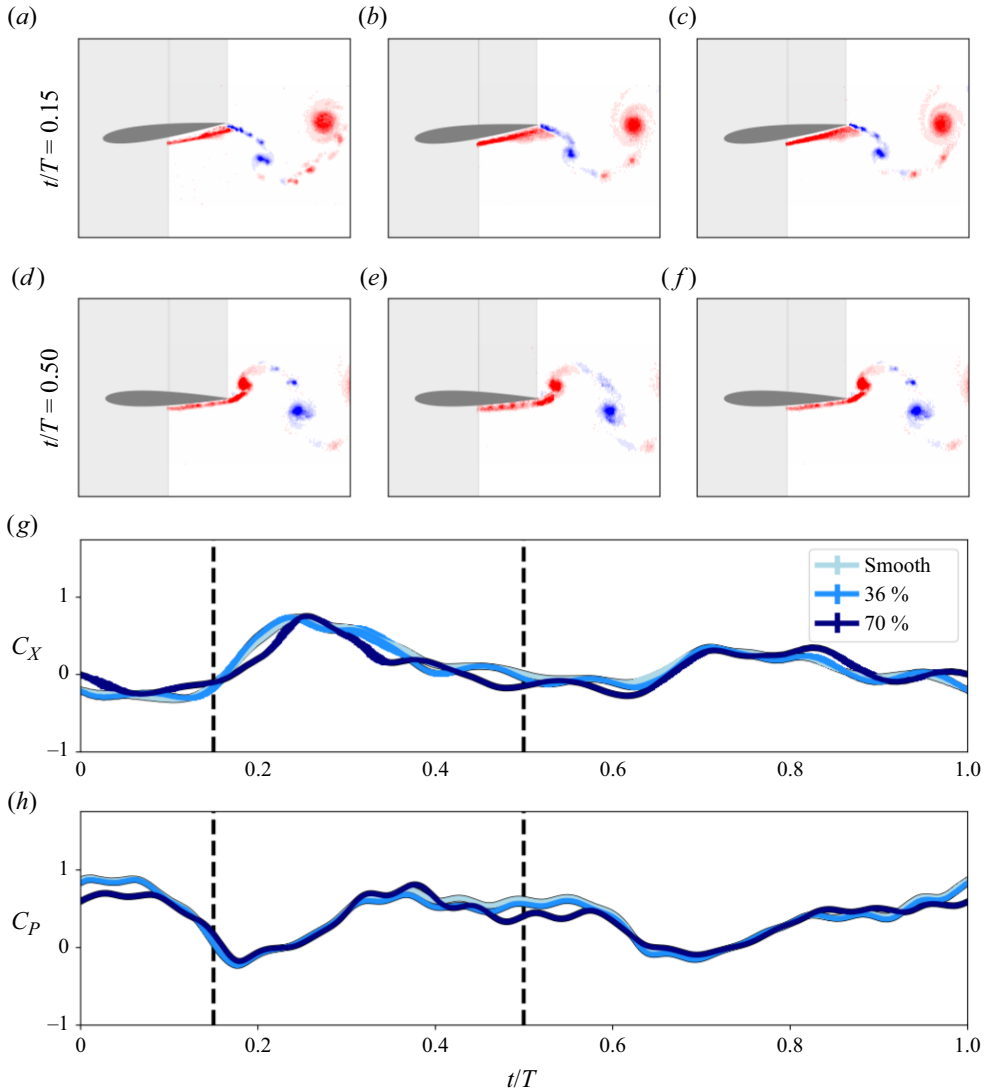


Figure 2. PIV results for $Re = 28000$: $t/T = 0.15$ (a–c) and $t/T = 0.50$ (d–f) for the smooth (a,d), 36% (b,e) and 70% (c,f). Instantaneous C_X (g) and instantaneous C_P (h). Panels (g,h) contain confidence intervals calculated as $CI = 4.6\sigma/\sqrt{N}$.

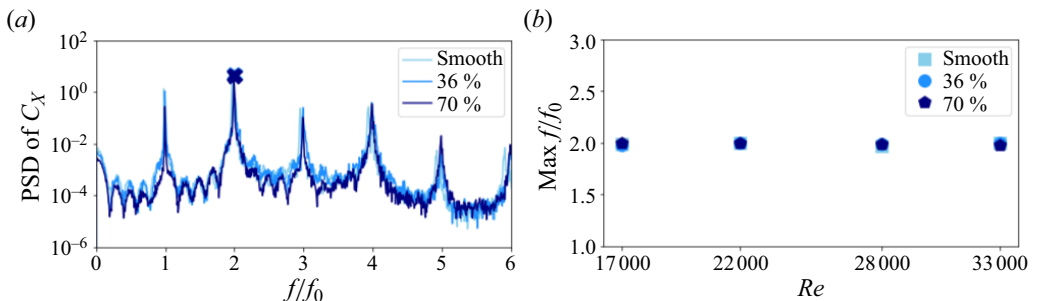


Figure 3. (a) Power spectral density analysis of the instantaneous C_X at $Re = 28000$. The cross indicates the location of the peak for each case. (b) Peak frequency across the Re values considered. A value of 2 denotes that the thrust force signal peak f is equal to twice the input pitching frequency f_0 .

Effects of roughness on the performance of pitching foils

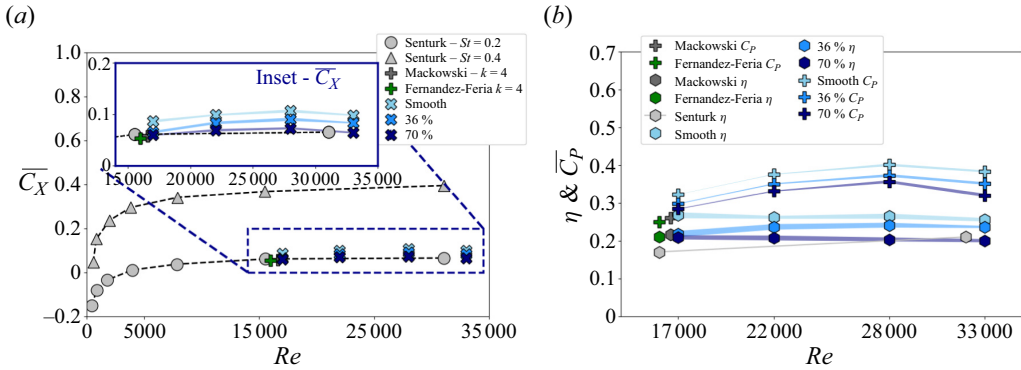


Figure 4. (a) Values of \overline{C}_X obtained in the current study (blue range) and compared with previous studies against Re : Senturk & Smits (2019) (grey). The data enclosed by the blue box present an inset of \overline{C}_X data for the Re range of $17\,000 \leq Re \leq 33\,000$. (b) Results of \overline{C}_P (hexagon) and η (cross) for current and previous studies: Mackowski & Williamson (2017) (dark grey) for $Re = 16\,600$, $k = 4$, $PP = 0c$ and $\theta_0 = 8^\circ$; Senturk & Smits (2019) (grey) for $500 \leq Re \leq 32\,000$, $St = 0.2-0.4$, $PP = 0.25c$ and $\theta_0 = 8^\circ$; Fernandez-Feria & Sanmiguel-Rojas (2020) for $Re = 16\,000$, $k = 4$, $PP = 0c$ and $\theta_0 = 8^\circ$. The shadow region introduces the confidence intervals calculated as $CI = 4.6\sigma/\sqrt{N}$.

highly dominated by f_0 , hence, by the kinematics. The dominant effects of the frequency and the kinematics on the development of the propulsive forces have been seen before. For example, Zurman-Nasution, Ganapathisubramani & Weymouth (2021) found that, compared with the flapping frequency and kinematics, shape-related parameters such as sweep angle have negligible effects on the propulsive performance. We believe that the influence of the rough elements is small compared with the effects that the kinematics and St have on the C_X and C_P evolutions.

Figure 4 presents the change in cycle-averaged performance coefficients for foils with different roughness coverages against Re . We compare our results with other NACA0012 studies conducted by Mackowski & Williamson (2017) ($Re = 16\,600$, $k = 4$), Senturk & Smits (2019) ($500 \leq Re \leq 32\,000$, $0.2 \leq St \leq 0.6$) and Fernandez-Feria & Sanmiguel-Rojas (2020) ($Re = 16\,000$, $4 \leq k \leq 60$). The thrust, \overline{C}_X , obtained for the smooth foil increases in the $17\,000 \leq Re \leq 28\,000$ range, in line with previous studies (Senturk & Smits 2019). The trend then reverses at $Re = 33\,000$. This change can be explained by looking at the evolution of the averaged-drag C_D calculated for a static foil at $\theta = 0$ (figure 5), where we observe a similar behaviour. The increase in the averaged C_D at $Re = 33\,000$ explains the decrease in \overline{C}_X reported for the pitching foil at figure 4. Nevertheless, the thrust values obtained in the current study fall within the findings by Senturk & Smits (2019) at $St = 0.2$ and $St = 0.4$. The main differences in the overall thrust production, higher in our study, can be associated with the effects of the pivot point location ($PP = 0.08c$ here and $PP = 0.25c$ in Senturk & Smits 2019), since as the PP moves towards the leading edge, a higher thrust production is expected (Mackowski & Williamson 2017). Finally, in the inset enclosed by a blue box, it is shown that \overline{C}_X decreases consistently with the addition of surface roughness across the Re range. In figure 4(b) we introduce the averaged power \overline{C}_P and efficiency η . For each roughness case, \overline{C}_P increases in the $17\,000 \leq Re \leq 28\,000$ range. The trend is then reversed, in line with the \overline{C}_X values. Regardless of the Re , we observe that an increase in roughness causes a decrease in \overline{C}_P . Regarding the efficiency, our results indicate higher η values than Mackowski & Williamson (2017), Fernandez-Feria & Sanmiguel-Rojas (2020) and Senturk & Smits

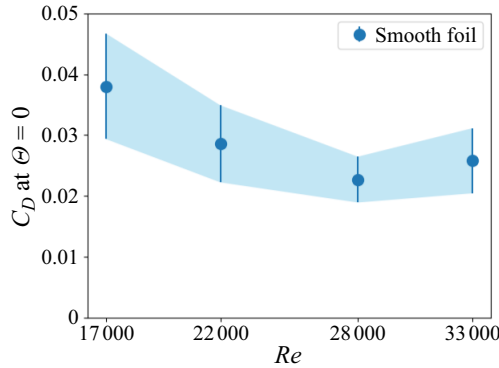


Figure 5. Averaged C_D values obtained for a static smooth foil at $\theta = 0^\circ$. The shadow region introduces the confidence intervals calculated as $CI = 4.6\sigma/\sqrt{N}$.

(2019), which could be due to differences in the pivot point location (at $x/c = 0.08$ distance from the leading edge in our study and at $x/c = 0.25$ distance in Senturk & Smits 2019), or the reduced frequency k ($k = 5.2$ here and $k = 4$ in Mackowski & Williamson 2017; Fernandez-Feria & Sanmiguel-Rojas 2020). We observe that any change in η with Re for the smooth case fall within the confidence intervals. Although Senturk & Smits (2019) point to an increase in η against increasing Re for a smooth pitching foil, other studies have reported a limited impact of Re on the propulsive performance of a pure-pitching foil for $Re \geq 8000$ (Deng *et al.* 2016). It might very well be a limitation of experimental measurements to delineate the difference in efficiency with increasing Reynolds number since it is a notoriously difficult quantity to measure accurately.

In relation to the rough foils, the efficiency also decreases as the surface roughness increases, similar to thrust and power. Although the flow fields show negligible alterations with the change in roughness, the cycle-averaged forces point to a performance reduction as the roughness increases. The thrust decrease observed for 36% and 70% roughness coverages compared with smooth foil can be related to an increase in the profile drag. To further explore this effect, in the next section, we have compared our flapping foil results with static foil measurements carried out using the same foils within the same Re range.

3.2. Comparison between static and flapping regimes

In this section, we introduce the data collected for static foils and compare it with the pitching foil results to further explore why there is a change in thrust production with a change in roughness coverage. The static data were acquired within the same Re range and roughness coverages as the flapping cases, for an angle of attack (θ) range of $-4^\circ \leq \theta \leq 20^\circ$. To compare both scenarios, we have selected an angle of attack value equal to the average θ experienced by the foil during half the pitching cycle (red dashed line in figure 6(a), denoted as θ_s). Next, we develop a comparison parameter or *penalty* that evaluates the change in streamwise force generated by the smooth and rough foils. Given that static state will produce drag (for all three foils) and the unsteady scenario will generate thrust, we present the penalty in its absolute value to help with the comparison. Since we have found surface roughness to be detrimental for $\overline{C_X}$ for all cases considered, a positive penalty value in the static state indicates an increase in drag due to roughness elements, whereas $Penalty > 0$ in the flapping regime means a decrease in thrust caused

Effects of roughness on the performance of pitching foils

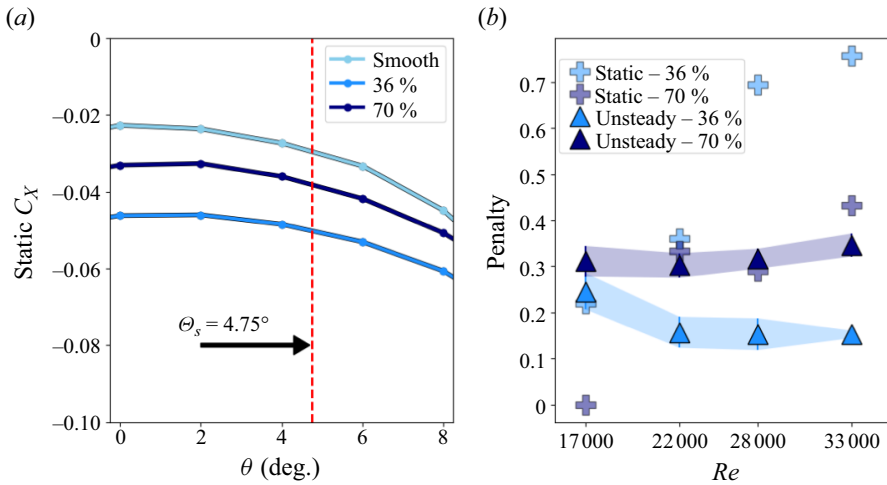


Figure 6. (a) Static C_x vs angle of attack θ measured using static foils at $Re = 28\,000$. Smooth foil is presented in light blue, 36% in medium blue and 70% in dark blue. The red dashed line indicates the θ used to compare with the unsteady regime, defined as $\theta_s = 4.75^\circ$. (b) Thrust and drag penalty due to roughness for both the flapping (triangles) and static results (crosses) for the 36% case (medium blue) and the 70% case (dark blue). The shadow region introduces the confidence intervals calculated as $CI = 4.6\sigma/\sqrt{N}$.

by the roughness elements. Here, *Penalty* is defined as the relative change in thrust for a rough foil compared with the smooth, $|(C_{X,rough} - C_{X,smooth})|/C_{X,smooth}$.

The penalty parameter is presented in figure 6 for static foil (crosses) and flapping foil measurements (triangles). The addition of surface roughness increases the drag production in the static state across the Re range considered. At $Re = 33\,000$, it reaches a 76% drag penalty for the 36% roughness and 43% penalty for the 70% roughness coverage, compared with the smooth foil. The drag performance of the foils at the static regime depends not only on the area covered by bumpers but also on the arrangement of the rough elements. Although the 70% presents more coverage than the 36%, the interactions between the flow and the intermittent distribution of the spanwise rows of rough elements at the 36% foil surface are responsible for the higher drag penalty. On the other hand, the flapping foils with roughness generate less thrust across the Re range compared with the smooth foil. At $Re = 33\,000$, the thrust decreases by 35% and 16% for 70% and 36% roughness coverages, respectively. However, the flapping state appears to be more robust to Re changes. It reduces the penalty observed for static foils, especially for the 36% coverage. At $Re = 33\,000$, foils with 36% coverage experiences a roughness penalty of 76% in the static state compared with a 16% penalty in the flapping state. Previous work has shown that parameters such as the kinematics or the Strouhal number have a strong influence on the propulsive performance of an oscillating foil (Zurman-Nasution *et al.* 2021). In line with this, we believe that the motion characteristics of this study could be minimising the impact of the roughness elements on both the wake development and force production.

To further analyse the data presented in figure 6, we present the out-of-plane vorticity (ω_z) in figure 7. The first row consists of the cycle-averaged unsteady pitching ω_z , and the positive vorticity regions are enclosed with isolines. In second and third rows, we present the flow-field data measured at $\alpha = 6^\circ$ for a pitching foil and a static foil, respectively. The first three columns correspond to 0% (smooth), 36% and 70% roughness coverages, respectively. The fourth column introduces a comparison between different roughness

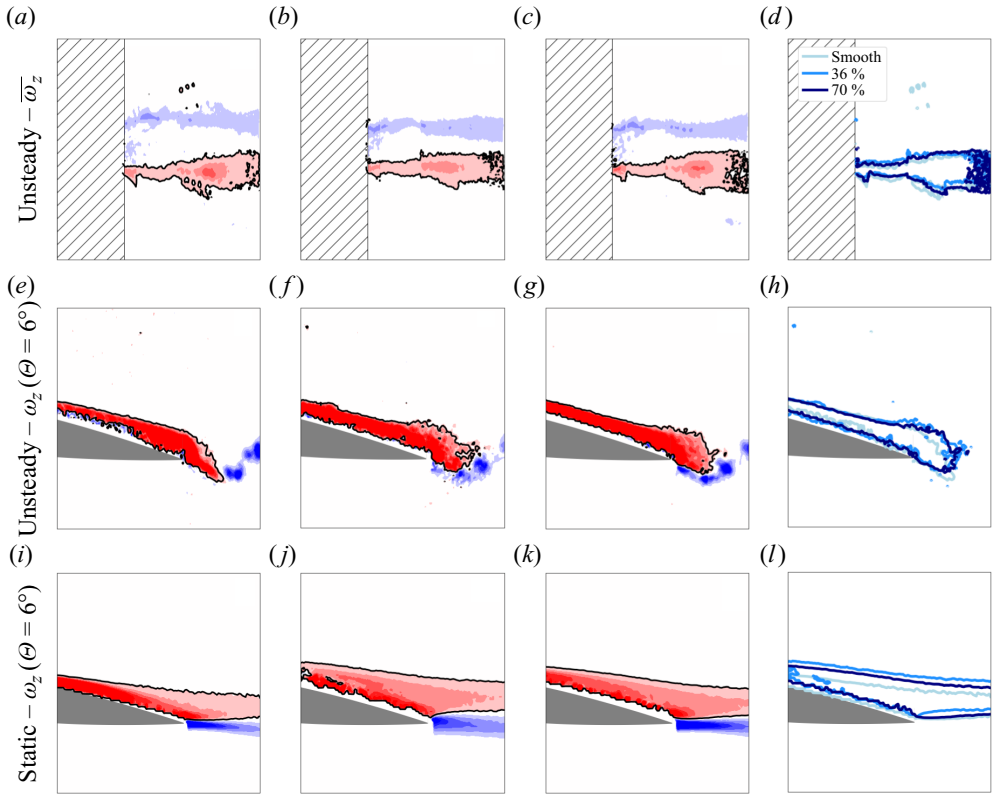


Figure 7. Pitching cycle-averaged vorticity (a–c), pitching instantaneous vorticity at $\theta = 6^\circ$ (e–g) and static PIV results at $\theta = 6^\circ$ (i–k). Smooth foil (a,e,i), 36% (b,f,j) and 70% (c,g,k). The comparison of the wakes generated by the foils at each of the conditions is presented at (d,h,l). All data obtained at $Re = 28\,000$.

cases with overlapped ω_z isolines. The comparison of all three flapping cases suggests that the addition of surface roughness does not introduce major changes in shedding shear layers. The mild effects could be explained considering the fact that the foils are operating at Reynolds numbers where the boundary layer is transitional (from laminar to turbulent). Adding roughness essentially induces an early development of a turbulent boundary layer, and it would be transitionally rough (if at all) in all these conditions. Hence, we would expect that increasing the size of the roughness elements could have a major impact on the wake characteristics of the pitching foil. In contrast, in the static state, foils with 36% and 70% roughness have thicker shear layer in time-average compared with the smooth case, similar to the findings by Guo *et al.* (2021). The presence of thicker shear layers, which are caused by the additional pressure drag incurred by the roughness elements, can be responsible for the 76% drag penalty shown in figure 6.

4. Conclusions

In this study, we have analysed the influence of surface roughness on the propulsive performance of flapping foils, using force and flow measurements. Three NACA0012 foils with different roughness coverage ratios have been constructed, and tested within the Reynolds number range of $17\,000 \leq Re \leq 33\,000$. We have found that the addition of surface roughness is detrimental to thrust production and efficiency of a pitching foil.

Effects of roughness on the performance of pitching foils

The foils with 36 % and 70 % roughness produce 16 % and 35 % less thrust, respectively, compared with the smooth foil. We have determined that Re does not play an important role in either the thrust or efficiency for the Re range and roughness coverage ratios considered. Although we have seen no significant change in the wake flow, the foils with roughness experience a decrease in thrust and efficiency, which can be explained by an increase in profile drag associated with the roughness elements. We have compared the effects of roughness on static and flapping states, finding that the former is considerably more sensitive to it. The roughness penalty for 36 % roughness coverage is reduced from 76 % in the static state to 16 % for flapping. The strongest decrease occurs at the highest Re , highlighting that the effect of roughness on flapping systems is very different than on static systems. This shows that the performance of flapping systems is more robust to the changes in surface roughness.





Supplementary movies. Supplementary movies are available at <https://doi.org/10.1017/jfm.2023.1009>.

Funding. This research was supported financially by the Office of Naval Research Global Award N62909-18-1-2091, the Engineering and Physical Sciences Research Council (Grant No: EP/R034370/1) and the doctoral training award.

Declaration of interests. The authors report no conflict of interest.

Data availability statement. All data supporting this study are openly available from the University of Southampton repository at <https://doi.org/10.5258/SOTON/D2943>.

Author ORCIDs.

-  Rodrigo Vilumbrales-Garcia <https://orcid.org/0000-0003-3778-0082>;
-  Melike Kurt <https://orcid.org/0000-0001-6711-7025>;
-  Gabriel D. Weymouth <https://orcid.org/0000-0001-5080-5016>;
-  Bharathram Ganapathisubramani <https://orcid.org/0000-0001-9817-0486>.

REFERENCES

- ACHENBACH, E. 1971 Influence of surface roughness on the cross-flow around a circular cylinder. *J. Fluid Mech.* **46** (2), 321–335.
- AFROZ, F., LANG, A., HABEGGER, M.L., MOTTA, P. & HUETER, R. 2016 Experimental study of laminar and turbulent boundary layer separation control of shark skin. *Bioinspir. Biomim.* **12** (1), 016009.
- ANDERSON, J.M., STREITLIEN, K., BARRETT, D.S. & TRIANTAFYLLOU, M.S. 1998 Oscillating foils of high propulsive efficiency. *J. Fluid Mech.* **360**, 41–72.
- BAKKEN, O.M., KROGSTAD, P.-Å., ASHRAFIAN, A. & ANDERSSON, H.I. 2005 Reynolds number effects in the outer layer of the turbulent flow in a channel with rough walls. *Phys. Fluids* **17** (6), 065101.
- BECHERT, D.W., BRUSE, M. & HAGE, W. 2000 Experiments with three-dimensional riblets as an idealized model of shark skin. *Exp. Fluids* **28** (5), 403–412.
- BECHERT, D.W., BRUSE, M., HAGE, W., VAN DER HOEVEN, J.G.T. & HOPPE, G. 1997 Experiments on drag-reducing surfaces and their optimization with an adjustable geometry. *J. Fluid Mech.* **338**, 59–87.
- BIXLER, G.D. & BHUSHAN, B. 2013 Fluid drag reduction with shark-skin riblet inspired microstructured surfaces. *Adv. Funct. Mater.* **23** (36), 4507–4528.
- CHOWDHURY, H., LOGANATHAN, B., WANG, Y., MUSTARY, I. & ALAM, F. 2016 A study of dimple characteristics on golf ball drag. *Procedia Engng* **147**, 87–91.
- DEAN, B. & BHUSHAN, B. 2010 Shark-skin surfaces for fluid-drag reduction in turbulent flow: a review. *Phil. Trans. R. Soc. A* **368** (1929), 4775–4806.
- DENG, J., SUN, L., TENG, L., PAN, D. & SHAO, X. 2016 The correlation between wake transition and propulsive efficiency of a flapping foil: a numerical study. *Phys. Fluids* **28** (9), 094101.
- DOMEL, A.G., DOMEL, G., WEAVER, J.C., SAADAT, M., BERTOLDI, K. & LAUDER, G.V. 2018a Hydrodynamic properties of biomimetic shark skin: effect of denticle size and swimming speed. *Bioinspir. Biomim.* **13** (5), 056014.

- DOMEL, A.G., SAADAT, M., WEAVER, J.C., HAJ-HARIRI, H., BERTOLDI, K. & LAUDER, G.V. 2018b Shark skin-inspired designs that improve aerodynamic performance. *J. R. Soc. Interface* **15** (139), 20170828.
- DU, Z., LI, H., CAO, Y., WAN, X., XIANG, Y., LV, P. & DUAN, H. 2022 Control of flow separation using biomimetic shark scales with fixed tilt angles. *Exp. Fluids* **63** (10), 1–12.
- EHRMANN, R.S., WILCOX, B., WHITE, E.B. & MANIACI, D.C. 2017 Effect of surface roughness on wind turbine performance. *Tech. Rep.* Sandia National Lab.(SNL-NM), Albuquerque, NM.
- FERNANDEZ-FERIA, R. & SANMIGUEL-ROJAS, E. 2020 Effect of the pivot point location on the propulsive performance of a pitching foil. *J. Fluids Struct.* **97**, 103089.
- GAD-EL HAK, M. & BUSHNELL, D.M. 1991 Separation control: review. *Trans. ASME J. Fluids Engng* **113**, 5–30.
- GUO, P., ZHANG, K., YASUDA, Y., YANG, W., GALIPON, J. & RIVAL, D.E. 2021 On the influence of biomimetic shark skin in dynamic flow separation. *Bioinspir. Biomim.* **16** (3), 034001.
- KURT, M. & MOORED, K.W. 2018 Flow interactions of two-and three-dimensional networked bio-inspired control elements in an in-line arrangement. *Bioinspir. Biomim.* **13** (4), 045002.
- MACKOWSKI, A.W. & WILLIAMSON, C.H.K. 2015 Direct measurement of thrust and efficiency of an airfoil undergoing pure pitching. *J. Fluid Mech.* **765**, 524–543.
- MACKOWSKI, A.W. & WILLIAMSON, C.H.K. 2017 Effect of pivot location and passive heave on propulsion from a pitching airfoil. *Phys. Rev. Fluids* **2** (1), 013101.
- MALLAH, S.R., SOORAJ, P., SHARMA, A. & AGRAWAL, A. 2021 Effect of superhydrophobicity on the wake of a pitching foil across various Strouhal numbers. *Phys. Fluids* **33** (11), 111905.
- MUSCUTT, L.E., WEYMOUTH, G.D. & GANAPATHISUBRAMANI, B. 2017 Performance augmentation mechanism of in-line tandem flapping foils. *J. Fluid Mech.* **827**, 484–505.
- OEFFNER, J. & LAUDER, G.V. 2012 The hydrodynamic function of shark skin and two biomimetic applications. *J. Expl Biol.* **215** (5), 785–795.
- SAGOL, E., REGGIO, M. & ILINCA, A. 2013 Issues concerning roughness on wind turbine blades. *Renew. Sust. Energy Rev.* **23**, 514–525.
- SCHNIPPER, T., ANDERSEN, A. & BOHR, T. 2009 Vortex wakes of a flapping foil. *J. Fluid Mech.* **633**, 411–423.
- SENTURK, U. & SMITS, A.J. 2019 Reynolds number scaling of the propulsive performance of a pitching airfoil. *AIAA J.* **57** (7), 2663–2669.
- VAN BOKHORST, E., DE KAT, R., ELSINGA, G.E. & LENTINK, D. 2015 Feather roughness reduces flow separation during low Reynolds number glides of swifts. *J. Expl Biol.* **218** (20), 3179–3191.
- WALSH, M. 1982 Turbulent boundary layer drag reduction using riblets. In *20th Aerospace Sciences Meeting*, p. 169. AIAA paper no 82-0169. AIAA.
- WEN, L., WEAVER, J.C. & LAUDER, G.V. 2014 Biomimetic shark skin: design, fabrication and hydrodynamic function. *J. Expl Biol.* **217** (10), 1656–1666.
- ZURMAN-NASUTION, A.N., GANAPATHISUBRAMANI, B. & WEYMOUTH, G.D. 2021 Fin sweep angle does not determine flapping propulsive performance. *J. R. Soc. Interface* **18** (178), 20210174.